Food Sci Biotechnol (2021) 30(4):531–539
https://doi.org/10.1007/s10068-021-00885-0

RESEARCH ARTICLE

Preparation and characterization of phytosterol-loaded nanoparticles with sodium caseinate/dextran conjugates

Feifan Li[1] · Xiaoli Wang[1] · Hongfu Wang[1] · Xiaohong Mei[1]

Received: 6 August 2020 / Revised: 10 January 2021 / Accepted: 26 January 2021 / Published online: 13 March 2021

Abstract Sodium caseinate (SC)/dextran conjugates were prepared via Maillard reaction under controlled dry-heating conditions. Moreover, the nanoparticles of phytosterols (PS) encapsulated by SC or SC/dextran were produced using the emulsion evaporation method. The encapsulation efficiency (78.81 ± 5.22%) of PS in SC/dextran nanoparticles was higher than that (73.5 ± 2.78%) in SC nanoparticles. Compared with the compact and dense structure of SC nanoparticles, SC/dextran nanoparticles existed as relatively loose aggregates. The result of differential scanning calorimetry demonstrated that the encapsulation of PS greatly decreased its crystallinity. The released rates of PS from SC and SC/dextran nanoparticles under acidic gastric conditions were 8.59% and 4.73%, respectively. After 7 h of intestinal digestion, the released rate (52.19%) of PS from SC/dextran nanoparticles was significantly higher than that from SC (32.67%) nanoparticles. Therefore, SC/dextran conjugates prepared by the Maillard reaction are more suitable to be used as wall material for the nano-encapsulation of PS.

Keywords Phytosterol · Sodium caseinate · Dextran · Glycosylation · Nanoparticle

✉ Xiaohong Mei
mxh@cau.edu.cn

Xiaoli Wang
942685139@qq.com

Hongfu Wang
1654093773@qq.com

[1] No. 17 Qinghua East Road, Haidian District, Beijing 100083, China

Abbreviations

PS	Phytosterol
SC	Sodium caseinate
DG	The degree of glycosylation
FTIR	Fourier transform infrared spectroscopy
SGF	Simulated gastric fluid
SIF	Simulated intestinal fluids

Introduction

Phytosterols, also called plant sterols (PS), resemble cholesterol in structural and biological functions (Maqsood et al., 2020; Mohammadi et al., 2020). Unlike cholesterol, PS cannot be synthesized de novo in the human body and must be obtained from the diets. The composition and content of PS differ in different plants, with the principal molecular species being β-sitosterol, stigmasterol, campesterol and brassicasterol (Moreau et al., 2002). Nuts, seeds, vegetable oils, cereals, and legumes are rich in PS (Flores and Ruiz Del Castillo, 2016). The cholesterol-lowering ability has been considered as the main function of PS (Nguyen, 1999). It is generally recognized that a daily intake of 2–3 g of PS can reduce LDL-cholesterol level by 10–15% (Katan et al., 2003; Normén et al., 2002).

However, poor solubility in water or oil and low bioaccessibility restrain the application of PS in food industry (Nguyen, 1999; Yang et al., 2016). Although the esterification of PS remarkably improves its solubility in the oil phase, excessive oil intake might cause health hazards. In the past decades, researchers tried to enhance the water solubility of PS through encapsulation technology. Furthermore, several kinds of delivery systems have been applied to load PS, including liposomes (Bagherpour et al., 2017), emulsions (Acevedo-Estupiñan et al., 2019),

nanoparticles (Cao et al., 2016). Among these delivery systems, protein-based nanoparticles have aroused extensive attention in recent years due to their easy preparation, high bioaccessibility, and acceptable compatibility (Cao et al., 2016). Some food-grade proteins, such as sodium caseinate (SC), soybean protein isolate (SPI), and whey protein isolate (WPI), have been used to prepare PS-loaded nanoparticles (Cao et al., 2016). However, the sensitivity of these proteins to pH variation and pepsin proteolysis hinder the further application of protein-based PS nanoparticles in food systems.

Although some physical and chemical modification methods can improve protein stability (Shen et al., 2017), most modified food proteins have potential health risks. By comparison, protein glycosylation is carried out under safe conditions, and obtained protein-polysaccharide conjugates effectively protect proteins from degradation due to steric hindrance of polysaccharide molecules (Zhang et al., 2015). Dextran is a neutral polysaccharide extensively used in the glycosylation of proteins. The main reason is that its neutral state inhibits the formation of electrostatic complexing between proteins and polysaccharides (Spotti et al., 2013). However, limited information is available concerning the properties of PS-loaded nanoparticles with protein-dextran conjugates and the release of PS in vitro.

In this study, the glycosylated SC with dextran was prepared by the Maillard reaction, and the obtained SC/dextran conjugates were characterized. And PS-loaded nanoparticles with SC or SC/dextran conjugates were produced by the emulsification-evaporation method, respectively. The physicochemical properties of the two nanoparticles, and the release kinetics of PS from the two nanoparticles, were compared, respectively. This experiment provided a basis for the application of SC/dextran conjugates in the encapsulation of PS.

Material and methods

Materials

Sodium caseinate (food grade) with 86.4% of protein content was obtained from New Zealand Fonterra Company (Auckland, New Zealand). Dextran with an average molecular weight of 40 kDa was purchased from Macklin Biochemical Technology Co., Ltd. (Shanghai, China). The mixture of PS, containing campesterol (24.8% of mass ratio), brassicasterol (1.0% of mass ratio), stigmasterol (26.6% of mass ratio), and β-sitosterol (43.4% of mass ratio), was purchased from Vita-Solar Biotechnology Co., Ltd. (Xian, China). Methyl-N-trimethyl silyl heptafluorobutylamide (MSHFBA) with 5% of 1-methylimidazole (1-MIN) were purchased from Sigma Chemical Co., Ltd. (Sintra, Portugal). Water purified by a Millipore purification system (Millipore, Milford, MS, USA) was used throughout the experiments. PS standards, including campesterol (65% purity), brassicasterol (95% purity), stigmasterol (95% purity), and beta-sitosterol (95% purity) were all purchased from Sigma-Aldrich Chemical Co., Ltd. (St. Louis, MO, USA). The reagents for quantity analysis of PS were of chromatographic grade, and other reagents were of analytical grade.

Preparation of SC/dextran conjugates

According to the previous method, SC/dextran conjugates were prepared by the Millard reaction with minor modifications (Corzo-Martínez et al., 2010). SC and dextran at a mass ratio of 1:5 were dissolved in Milli-Q water with constant agitation, and then the pH value was adjusted to 7.0 with 0.1 M NaOH. The sample was freeze-dried, and the obtained lyophilized powders were incubated in a desiccator over a saturated KBr solution (79% relative humidity) for 6, 12, 24, 36, 48, and 60 h at 60 °C, respectively. The samples were separately collected at 6, 12, 24, 36, 48, and 60 h and stored at − 20 °C for further use.

Characterization of SC/dextran conjugates

The free amino groups were measured by the OPA method to evaluate the extent of the Maillard reaction (de Oliveira et al., 2016). 200 μL of the samples were mixed with 4 mL OPA reagent and then incubated at 25 °C for 5 min. The absorbance was measured at 340 nm using a Microplate reader (Varioskan Flash, Thermo Electron, USA). The degree of glycosylation (DG) was calculated according to the following formula:

$$\mathrm{DG} = \frac{A_0 - A_t}{A_0} \quad (1)$$

where A_0 is the absorbance value before heating and A_t is the absorbance value after heating for t min.

The SC/dextran conjugates were confirmed by SDS-PAGE using 5% stacking gel and 12% separating gel (Mohamed et al., 2007). After electrophoresis, the gel was stained with the Coomassie Brilliant Blue R-250, and then faded with 10% acetic acid and 10% ethanol.

The conformations of SC, SC/dextran, and dextran were measured by the Fourier transform spectrophotometer (Spectrum 100, Perkin-Elmer, Warrington, UK). 2.0 mg of the samples were mixed with 200 mg of potassium bromide (KBr), and then the mixtures were pressed into the pellet and placed in the sample holder. The spectra were scanned from 4000 to 400 cm^{-1} wavenumbers in 32 scans with a 4 cm^{-1} resolution. The data were analyzed using

OMNIC 8.2 software (Thermo Fisher Scientific Inc., Waltham, MS, USA).

The surface morphology of SC/dextran conjugates was observed by a field emission scanning electron microscope (FE-SEM, SU8010, Hitachi, Japan) at an accelerating voltage of 3.0 kV. Prior to the observation, the surfaces of the samples were sputter-coated with a gold layer to avoid charging under the electron beam.

Preparation of PS-loaded nanoparticles

PS-loaded nanoparticles were prepared according to the method described by Leong et al. (2011) with a few modifications. SC/dextran and SC were dissolved in Milli-Q water (1.0%, w/v), respectively. The pH values were then adjusted to 7.0 using 0.1 M NaOH with continuous stirring for 2 h to ensure complete hydration. At the same time, PS was dissolved in ethanol at a concentration of 1% (w/v). The ethanol solution containing PS was added to the aqueous solution containing SC/dextran or SC in a volume ratio of 1:10 under vigorous mixing conditions (11,000 × g, 2 min) using a high-speed disperser (T100, PhD Technology LLC, China). The above coarse emulsion was further emulsified using an ultrasonicator at 250 W for 25 min (SCIENTZ-IID, Ningbo, China). The obtained emulsion was evaporated by a rotary evaporator at 40 °C to remove ethanol. Some part of the resultant dispersion containing PS-loaded nanoparticles was stored at 4 °C. The other part was freeze-dried and the lyophilized powders were kept at − 20 °C for further use.

Measurement of particle size and zeta potential

Size, polydispersity index (PDI), and zeta potential of PS-loaded nanoparticles were determined by dynamic light scattering using Zetasizer Nano-ZS90 (Malvern Instruments Ltd., UK) (Shen et al., 2017). The nanoparticles were diluted 100-fold with Milli-Q water before measurement. All the experiments were performed at 25 °C.

Differential scanning calorimetry (DSC)

The thermal transitions of the dried samples including SC/dextran, free PS and PS-loaded nanoparticles were investigated using a DSC-60 differential scanning calorimeter (Shimadzu Corporation, Japan). 5–10 mg of the samples were sealed in aluminum pans and heated from 30 to 250 °C at a scan rate of 10 °C/min. The nitrogen flow was set at 25 mL/min. An empty pan was used as the control.

In vitro release of PS-loaded nanoparticles

The release trend of PS from the nanoparticles was investigated by the simulated gastric fluid (SGF: 3.2 mg/mL pepsin, 2.0 mg/mL NaCl, pH 2.0) and simulated intestinal fluids (SIF: 10 mg/mL bile salt, 0.4 mg/mL lipase, 6.8 mg/mL K_2HPO_4, 5 mM $CaCl_2$, pH 8.0) according to Scheuble et al. (2018) with minor modifications.

Five mL of the PS-loaded nanoparticles were placed into a dialysis bag (8–14 kDa, Solarbio, China) and immersed into 150 mL of the SGF. The above system was incubated at 37 ± 1 °C for 2 h, and then the released content of PS was measured as described in the section of "Quantity analysis of PS". Using the same system, the release trend was measured in SIF conditions by immersing the dialysis bag into 150 mL of the SIF. Incubation was maintained at 37 ± 1 °C for 7 h, and 2 mL of buffer solution was taken out as the sample in the time intervals of 1 h. The removed solution was then replaced with fresh SIF. The PS content in the collected samples were measured as described in the section of "Quantity analysis of PS".

The PS release (%) in SGF was calculated as the following equation:

$$\text{PS release}\ (\%) = \frac{M_1}{M_0} \times 100\% \tag{2}$$

where M_1 is the amount of the released PS at the end of simulated gastric digestion, M_0 is the total amount of PS loaded in the nanoparticles.

The PS release (%) in SIF was calculated as the following equation:

$$\text{PS release}\ (\%) = \frac{M_t}{M_0 - M_1} \times 100\% \tag{3}$$

where M_t is the amount of the released PS at time t.

According to the method described by Ganje et al. (2019), different experimental models were used to evaluate the effective release mechanism of PS from SC and SC/dextran nanoparticles in SIF.

Quantity analysis of PS

100 µL of 5α-cholestane (1.0 g/mL) and 5 mL of ethanolic KOH (1 M) were separately added into 1 mL of the sample, and the mixture was saponified (Chiou et al. 2009).

The unsaponifiable samples were silylated with 100 µL of MSHFBA /1-MIN (95:5, v/v) at 75 °C for 20 min and dissolved into 1 mL of n-hexane. Then they were analyzed using a 6890 N GC system coupled to a 5973 Mass Selective Detector (Agilent Technologies, USA). 1.0 µL of the sample was injected into the GC, equipped with a capillary column (DB-5MS, 30 m × 0.25 mm × 0.25 µm;

Agilent Technologies, USA) (He et al., 2019). Helium was used as the carrier gas at a flow rate of 1.2 mL/min. The chromatographic conditions were as follows: initial oven temperature was maintained for 1 min at 100 °C and subsequently programmed from 100 to 290 °C at a rate of 10 °C/min and then held for 10 min. The sample was injected in splitless mode. The ion source temperatures, and transmission line were set at 250 °C and 290 °C, respectively. The amount of PS was calculated using the following formula:

$$\text{The amount of PS } (\mu g) = \Sigma \frac{PA_i \times m_s}{PA_s} \quad (4)$$

where PA_i means the peak area of each PS (including campesterol, brassicasterol, stigmasterol, and β-sitosterol), PA_s means the peak area of the internal standard, and m_s means the amount (μg) of the internal standard.

Statistical analysis

All the experiments were conducted in triplicate with data reported as the mean ± standard deviation. Experimental statistics were analyzed by analysis of variance (ANOVA) with the SPSS17.0 software (IBM Corporation, USA). Duncan's multiple range test was used to determine the significant differences between mean values. The significance was defined at the 95% confidence level.

Results and discussion

Characterization of SC–dextran conjugates

In this study, DG was used to evaluate the degree of the Millard reaction between SC and dextran. As shown in Fig. 1A, the DG of SC/dextran conjugates significantly increased from 6 to 36 h ($P < 0.05$), illustrating that free amines located on the surface of SC could react with the carbonyl groups of dextran easily at the early stage of the Millard reaction (Zhang et al., 2015). However, with a prolonged time, the DG of the conjugates remained stable. This phenomenon suggested that steric hindrance of the polysaccharides restrained further glycosylation (Huang et al., 2020).

SDS-PAGE was performed to confirm the formation of SC/dextran conjugates, and the results are indicated in Fig. 1B. Two feature bands in lane 1 (25–35 kDa and 35–40 kDa) were clearly observed, which were respectively identified as α-casein and β-casein (Böttger et al., 2019). The band distribution in lane 2 was the same as lane 1, demonstrating that the simple blend of SC and dextran did not lead to the formation of SC/dextran conjugates. Compared with lane 1 and 2, the native bands for α-casein and β-casein in lane 3 became slightly lighter, and the broad diffusive and smeared bands were found in the area of higher molecular weights, indicating the formation of SC/dextran conjugates. The similar results were also reported in other studies (Fechner et al., 2007; Consoli et al., 2018).

The FTIR spectra of SC, dextran and SC/dextran conjugates are shown in Fig. 1C. In the region between 3500 and 3000 cm^{-1}, O–H stretching vibration caused the broad absorption peaks of the three samples. Additionally, the absorption peaks at 3000–2800 cm^{-1} corresponded to the C–H stretching vibration of the three samples. In comparison with the spectrum of SC, the peak positions of the two stretching vibrations (O–H and C–H) in SC/dextran were varied, accompanied by the increasing absorbance of hydroxyl and saturated C–H groups, demonstrating the formation of covalent complexation between SC and dextran (Hadidi et al., 2020). The other two characteristic peaks of SC were observed at 1659.5 and 1516.3 cm^{-1}, which were attributed to amide I band (1700–1600 cm^{-1}) and amide II band (1600–1500 cm^{-1}), respectively (Miller et al., 2013). After glycosylation, the transmittance of amide I band was strengthened, and the peak of amide II band was shifted from 1659 to 1657 cm^{-1}. This phenomenon implied the introduction of dextran and Maillard reaction led to the variation of the secondary structure of SC (Liu et al., 2014; Vergne et al., 2017).The absorption peaks at 904 cm^{-1} and 757 cm^{-1} in SC/dextran were considered as the characteristic of glucose residues (Zhu et al., 2016).

As shown in Fig. 1D, SC particles exhibited a spherical-like shape with a smooth surface. However, the conjugates had an irregular broken lamellar structure, which might be due to the destruction of SC structure caused by the covalent binding of dextran to SC. Additionally, the surface structure of the conjugates became loose and porous, indicating the covalent combination of SC and dextran molecules led to the formation of inhomogeneous and accumulated structure (Gupta et al., 2018).

Characterization of PS nanoparticles-based SC and SC/dextran

As shown in Table 1 and Fig. 2A, the PDI values of PS-loaded nanoparticles based on SC and SC/dextran conjugates are around 0.2, indicating that both nanoparticles exhibited unimodal particle diameter distributions.

The particle diameter of PS-loaded nanoparticles based on SC/dextran is obviously larger than that of PS nanoparticles based on SC, which might be due to the addition of dextran. In addition, SC-based nanoparticles had negative zeta potential (− 19.6 ± 0.23 mV), which was attributed to SC carrying a negative charge at pH

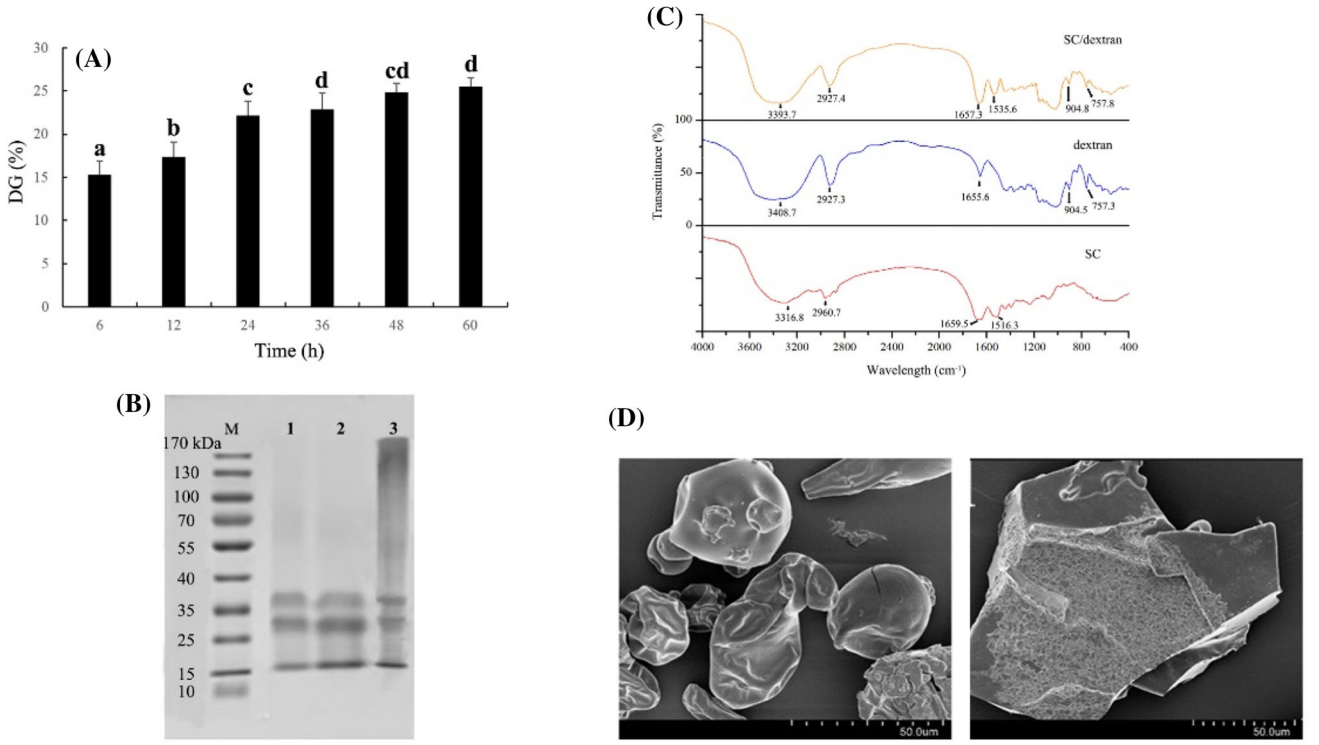

Fig. 1 Characterization of SC/dextran conjugates. (**A**) DG of SC/dextran conjugates (n = 3). (**B**) SDS-PAGE of protein marker (M), SC (1), the mixture of SC and dextran (2), SC/dextran conjugates (3). (**C**) FTIR spectra of SC, dextran and SC/dextran. (**D**) SEM images of SC (left) and SC/dextran conjugates (right)

Table 1 Mean particle diameter, PDI, Zeta-potential, and encapsulation efficiency of PS for the nanoparticles with SC and SC/dextran (n = 3)

Sample	Mean particle diameter (nm)	PDI	Zeta –potential (mV)	Encapsulation efficiency (%)
SC	252.67 ± 3.60^{A}	0.18 ± 0.03^{A}	-19.6 ± 0.23^{A}	73.50 ± 2.78^{A}
SC/dextran	283.73 ± 14.70^{B}	0.22 ± 0.01^{A}	-24.7 ± 0.16^{B}	78.81 ± 5.22^{A}

The values were expressed as means ± standard derivations. Different letters in the same column represented significant differences between groups ($P < 0.05$)

higher than its isoelectric point (approximately 4.6) (Consoli et al., 2018). Although SC/dextran conjugates encapsulating nanoparticles also showed a negative charge, the absolute value of zeta potential was significantly higher than that of SC-based nanoparticles. This phenomenon suggested that the decrease in the number of NH_2 amino groups led to higher negative charge density and higher electrostatic repulsion (Huang et al., 2020). The encapsulation efficiency of PS was 73.5 ± 2.78% and 78.81 ± 5.22% in native SC and SC/dextran nanoparticles, respectively. The higher encapsulation efficiency in SC/dextran nanoparticles might be attributed to the exposure of hydrophobic patches on protein surface during the glycosylation, increasing the binding ability of the glycosylated protein to hydrophobic PS (Morgan et al., 2001).

SEM of PS nanoparticles based on SC and SC/dextran conjugates are shown in Fig. 2B, C. Both SC and SC/dextran nanoparticles appeared to be spherically shaped. SC nanoparticles exhibited a compact and dense structure. However, SC/dextran nanoparticles existed as relatively loose aggregates, and the obvious pores among the aggregates were observed, suggesting that the steric barriers caused by glycosylation partly limited the formation of protein aggregation.

The thermal properties of free PS and freeze-dried PS nanoparticles over a broad temperature range (25–250 °C) are shown in Fig. 3. The free PS separately exhibited a broad endothermic peak at 123.3 °C and a sharp endothermic peak at 144.2 °C, indicating that the PS molecules existed in different crystal forms (Christiansen et al., 2002). However, no endothermic peaks were observed in the PS nanoparticles based on SC and SC/dextran, demonstrating that the encapsulation of PS into

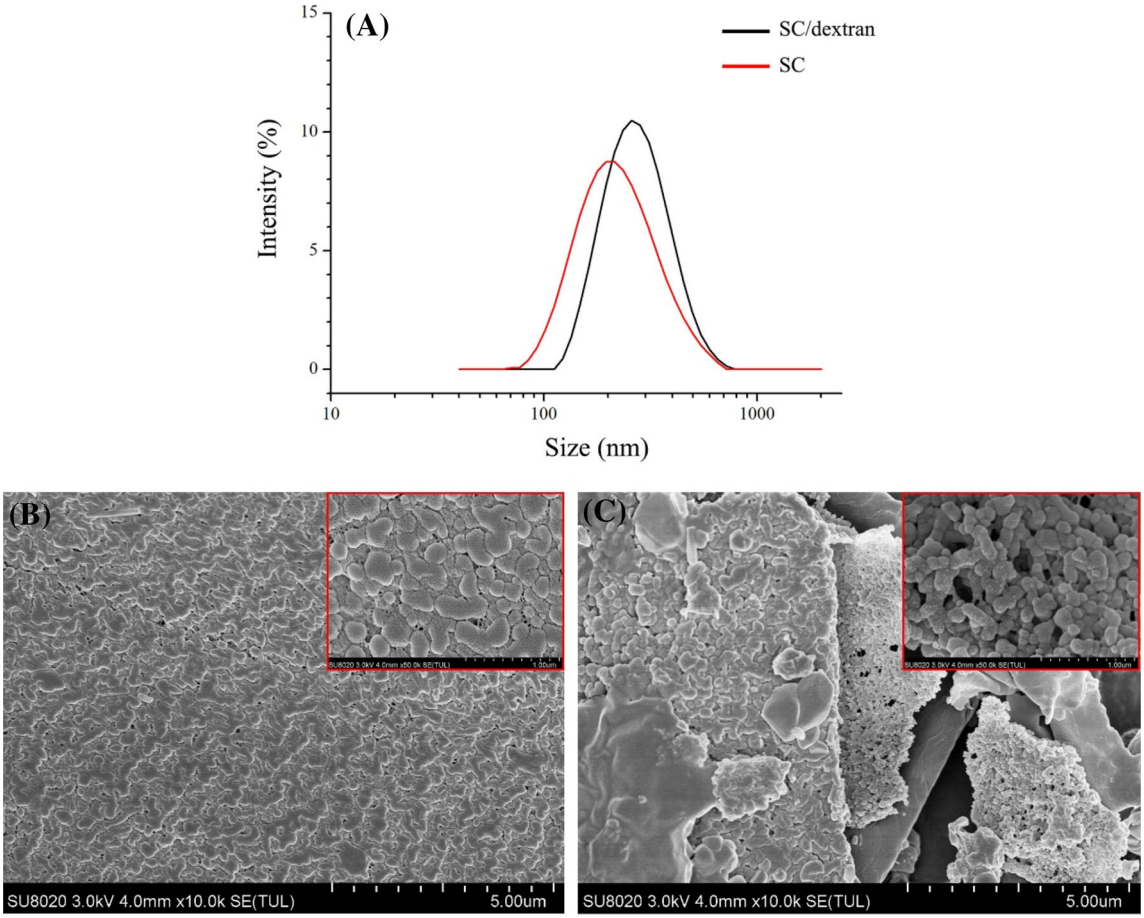

Fig. 2 Diameter distribution of PS nanoparticles (**A**); SEM images of PS nanoparticles with SC (**B**) and SC/dextran (**C**), the box indicated relevant samples in smaller scale

Figure. 3. DSC profiles of PS and freeze-dried PS nanoparticles

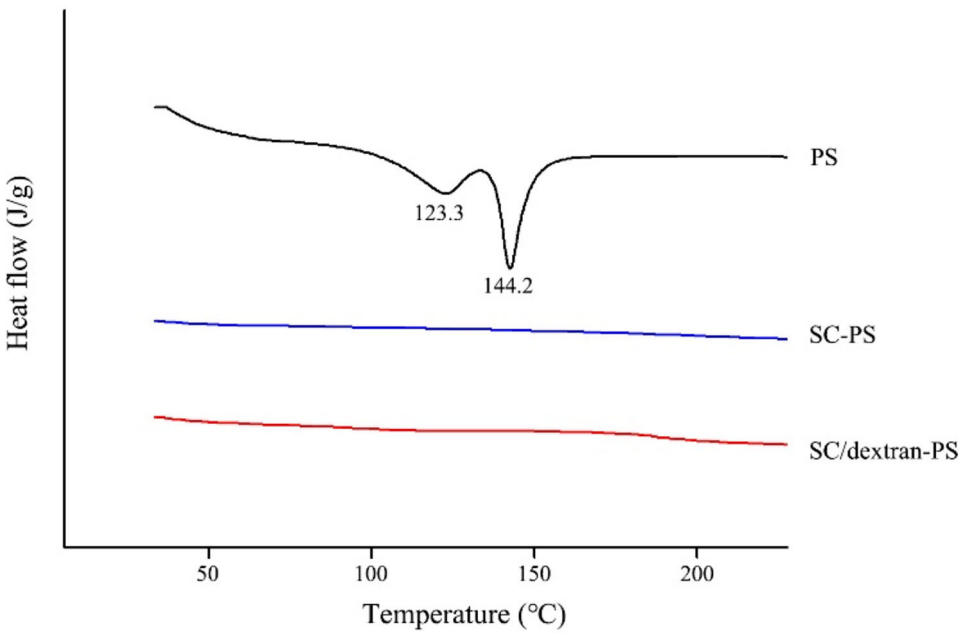

nanoparticles remarkably decreased its crystallinity (Cao et al., 2016).

PS release during in vitro digestion

As shown in Fig. 4A, the total release of PS in SGF was 8.59% for SC-based PS nanoparticles and 4.73% for SC/dextran-based PS nanoparticles. The lower released rate of PS from SC/dextran nanoparticles demonstrated that the glycosylation between SC and dextran might partly protect SC against acidic and enzymatic hydrolysis. Thus, more PS was retained inside the SC/dextran nanoparticles and absorbed in the gut, which led to higher bioavailability of PS (Flores and Kong, 2017).

The release trend of PS from SC-based and SC/dextran-based nanoparticles in SIF is shown in Fig. 4B. After 7 h of digestion, the accumulative amount of released PS from SC-based and SC/dextran-based nanoparticles was separately 32.67% and 52.19%, suggesting PS release was promoted by glycosylation. One possible explanation is that the surface structure of PS nanoparticles with SC/dextran conjugates was loose and porous, increasing contact area between the nanoparticles and digestion fluids, which made PS encapsulated inside the nanoparticles easier to be released.

Additionally, the release mechanisms of PS in SIF were illustrated using the mathematical models in Table 2. For the coefficients of determination, the release kinetics of PS from the two kinds of nanoparticles was best described by Peppas model ($R^2 > 0.95$). The value of n in Peppas model is below 0.43, indicating the release process was dominated by the Fickian diffusion in both SC and SC/dextran-based nanoparticles (Lao et al., 2011). Mostly the "shell" structure consisted of SC or SC/dextran nanoparticles could not be swelled or deconstructed, thus leading to the continuous release of PS during digestion. Similar results were also found in other delivery systems (Flores and Kong, 2017; Ganje et al., 2019).

Table 2 Release kinetic models and parameters of PS

Model	Equation	Parameter	SC	SC/dextran
Zero order	$C = Kt + b$	K	0.0386	0.0600
		b	0.1004	0.1835
		R^2	0.7686	0.7136
First order	$C = e^{Kt} + b$	K	0.0332	0.0480
		b	− 0.8911	− 0.7966
		R^2	0.7441	0.6763
Peppas	$C = Kt^{0.5}$	K	0.1803	0.3236
		n	0.3133	0.2594
		R^2	0.9698	0.9762
Higuchi	$C = Kt^n$	K	0.1362	0.2258
		R^2	0.7167	0.3602

C: the amount of released phytosterol at the given time t; k and b: kinetic constant; n: release exponent

In this study, SC/dextran conjugates were successfully prepared by the Maillard reaction. Both SC-based and SC/dextran-based nanoparticles effectively inhibited the crystallinity of PS. Furthermore, SC/dextran-based nanoparticles showed better properties in the encapsulation of PS, such as higher encapsulation efficiency, improved gastric acid resistance and higher release rate in SIF. Therefore, SC/dextran-based nanoparticles are more suitable to be used as a controlled-release PS delivery system.

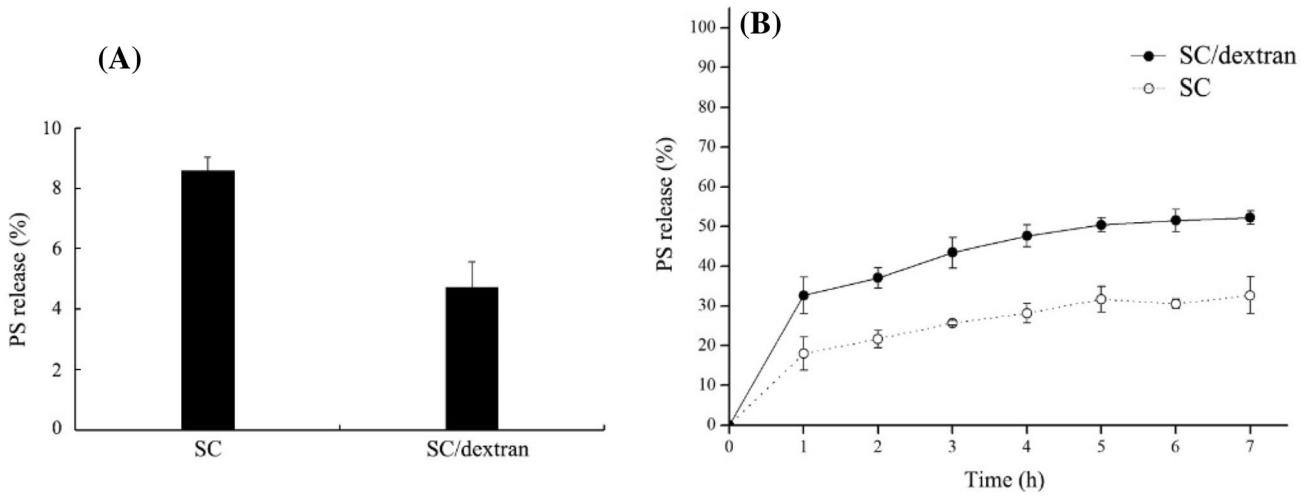

Fig. 4 In vitro release of PS from the nanoparticles in SGF (**A**) and SIF (**B**). All experiments were conducted in triplicate

Acknowledgements This study was supported by the Special Project of Agriculture Produce Quality Safety Risk Assessment (GJFP2019042) from Ministry of Agriculture and Rural Affairs of the People's Republic of China.

Compliance with ethical standards

Conflict of interest The authors declare that they have no known competing financial interests or personal relationships that could have influenced the work reported in this paper.

References

Acevedo-Estupiñan MV, Gutierrez-Lopez GF, Cano-Sarmiento C, Parra-Escudero CO, Rodriguez-Estrada MT, Garcia-Varela R, García HS. Stability and characterization of O/W free phytosterols nanoemulsions formulated with an enzymatically modified emulsifier. LWT-Food Science and Technology 107: 151-157 (2019)

Bagherpour S, Alizadeh A, Ghanbarzadeh S, Mohammadi M, Hamishehkar H. Preparation and characterization of beta-sitosterol-loaded nanostructured lipid carriers for butter enrichment. Food Bioscience 20: 51-55 (2017)

Böttger F, Dupont D, Marcinkowska D, Bajka B, Mackie A, Macierzanka A. Which casein in sodium caseinate is most resistant to *in vitro* digestion? Effect of emulsification and enzymatic structuring. Food Hydrocolloids 88: 114-118 (2019)

Cao W, Ou S, Lin W, Tang C. Food protein-based phytosterol nanoparticles: fabrication and characterization. Food & Function 7: 3973-3980 (2016)

Chiou A, Kalogeropoulos N, Salta FN, Efstathiou P, Andrikopoulos NK. Pan-frying of french fries in three different edible oils enriched with olive leaf extract: oxidative stability and fate of microconstituents. LWT - Food Science and Technology 42: 1090-1097 (2009)

Christiansen LI, Rantanen JT, Bonsdorff AKv, Karjalainen MA, Yliruusi JK. A novel method of producing a microcrystalline β-sitosterol suspension in oil. European Journal of Pharmaceutical Sciences 15: 261-269 (2002)

Consoli L, Dias RO, Rabelo RS, Furtado GF, Sussulini A, Cunha RL, Hubinger MD. Sodium caseinate-corn starch hydrolysates conjugates obtained through the Maillard reaction as stabilizing agents in resveratrol-loaded emulsions. Food Hydrocolloids 84: 458-472 (2018)

Corzo-Martínez M, Soria AC, Belloque J, Villamiel M, Moreno FJ. Effect of glycation on the gastrointestinal digestibility and immunoreactivity of bovine β-lactoglobulin. International Dairy Journal 20: 742-752 (2010)

de Oliveira FC, Coimbra JS, de Oliveira EB, Zuniga AD, Rojas EE. Food protein-polysaccharide conjugates obtained via the Maillard reaction: A review. Critical Reviews In Food Science and Nutrition 56: 1108-1125 (2016)

Fechner A, Knoth A, Scherze I, Muschiolik G. Stability and release properties of double-emulsions stabilised by caseinate–dextran conjugates. Food Hydrocolloids 21: 943-952 (2007)

Flores FP, Kong F. *In vitro* release kinetics of microencapsulated materials and the effect of the food matrix. Annual Review of Food Science and Technology 8: 237-259 (2017)

Flores G, Ruiz Del Castillo ML. Cancer-related constituents of strawberry jam as compared with fresh fruit. Cancers (Basel) 8: 16 (2016)

Ganje M, Jafari SM, Tamadon AM, Niakosari M, Maghsoudlou Y. Mathematical and fuzzy modeling of limonene release from amylose nanostructures and evaluation of its release kinetics. Food Hydrocolloids 95: 186-194 (2019)

Gupta C, Arora S, Syama MA, Sharma A. Physicochemical characterization of native and modified sodium caseinate- Vitamin A complexes. Food Research International 106: 964-973 (2018)

Hadidi M, Pouramin S, Adinepour F, Haghani S, Jafari SM. Chitosan nanoparticles loaded with clove essential oil: Characterization, antioxidant and antibacterial activities. Carbohydrate Polymers 236: 116075 (2020)

He W, Li L, Wang H, Rui J, Cui D. Synthesis and cholesterol-reducing potential of water-soluble phytosterol derivative. Journal of Functional Foods 60: 103428 (2019)

Huang G, Wang H, Wang F, Du Y, Xiao J. Maillard reaction in protein - polysaccharide coacervated microcapsules and its effects on microcapsule properties. International Journal of Biological Macromolecules 155: 1194-1201 (2020)

Katan MB, Grundy SM, Jones P, Law M, Miettinen T, Paoletti R. Efficacy and safety of plant stanols and sterols in the management of blood cholesterol levels. Mayo Clinic Proceedings 78: 965-978 (2003)

Lao LL, Peppas NA, Boey FY, Venkatraman SS. Modeling of drug release from bulk-degrading polymers. International Journal of Pharmaceutics 418: 28-41 (2011)

Leong WF, Lai OM, Long K, Che Man YB, Misran M, Tan CP. Preparation and characterisation of water-soluble phytosterol nanodispersions. Food Chemistry 129: 77-83 (2011)

Liu Q, Kong B, Han J, Sun C, Li P. Structure and antioxidant activity of whey protein isolate conjugated with glucose via the Maillard reaction under dry-heating conditions. Food Structure-Netherlands 1: 145-154 (2014)

Maqsood S, Adiamo O, Ahmad M, Mudgil P. Bioactive compounds from date fruit and seed as potential nutraceutical and functional food ingredients. Food Chemistry 308: 125522 (2020)

Miller LM, Bourassa MW, Smith RJ. FTIR spectroscopic imaging of protein aggregation in living cells. Biochimica et Biophysica Acta 1828: 2339-2346 (2013)

Mohamed A, Hojilla-Evangelista MP, Peterson SC, Biresaw G. Barley protein isolate: Thermal, functional, rheological, and surface properties. Journal of the American Oil Chemists Society 84: 281-288 (2007)

Mohammadi M, Jafari SM, Hamishehkar H, Ghanbarzadeh B. Phytosterols as the core or stabilizing agent in different nanocarriers. Trends in Food Science & Technology 101: 73-88 (2020)

Moreau RA, Whitaker BD, Hicks KB. Phytosterols, phytostanols, and their conjugates in foods: Structural diversity, quantitative analysis, and health-promoting uses. Progress in Lipid Research 41: 457-500 (2002)

Morgan F, Molle D, Henry G, Venien A, Leonil J, Peltre G, Levieux D, Maubois JL, Bouhallab S. Glycation of bovine β-Lactoglobulin: effect on the protein structure. International Journal of Food Science & Technology 34: 429-435 (2001)

Nguyen. The cholesterol-lowering action of plant stanol esters. The Journal of Nutrition 129: 2109-2112 (1999)

Normén L, Bryngelsson S, Johnsson M, Evheden P, Ellegård L, Brants H, Dutta P. The phytosterol content of some cereal foods commonly consumed in Sweden and in the Netherlands. Journal of Food Composition & Analysis 15: 693-704 (2002)

Scheuble N, Schaffner J, Schumacher M, Windhab EJ, Liu D, Parker H, Fischer P. Tailoring emulsions for controlled lipid release: Establishing *in vitro–in vivo* correlation for digestion of lipids. ACS Applied Materials & Interfaces 10: 17571-17581 (2018)

Shen X, Zhao C, Guo M. Effects of high intensity ultrasound on acid-induced gelation properties of whey protein gel. Ultrasonics Sonochemistry 39: 810-815 (2017)

Spotti MJ, Perduca MJ, Piagentini A, Santiago LG, Rubiolo AC, Carrara CR. Does dextran molecular weight affect the mechanical properties of whey protein/dextran conjugate gels? Food Hydrocolloids 32: 204-210 (2013)

Vergne DMC, Vasconcelos ACP, Batista RA, Freitas MM, Júnior RLCA, de Freitas O, Cardoso JC. Collagen modification by Maillard reaction. Journal of Thermal Analysis and Calorimetry 131: 671-679 (2017)

Yang F, Oyeyinka SA, Ma Y. Novel synthesis of phytosterol ester from soybean sterol and acetic anhydride. Journal of Food Science 81: 1629-1635 (2016)

Zhang B, Guo X, Zhu K, Peng W, Zhou H. Improvement of emulsifying properties of oat protein isolate–dextran conjugates by glycation. Carbohydrate Polymers 127: 168-175 (2015)

Zhu W, Xue X, Zhang Z. Ultrasonic-assisted extraction, structure and antitumor activity of polysaccharide from Polygonum multiflorum. International Journal of Biological Macromolecules 91: 132-142 (2016)